

Relationship between magnetic asymmetry and magnetization in ultrafast transverse magneto-optical Kerr effect spectroscopy in the extreme ultraviolet spectral range

Johanna Richter ¹, Somnath Jana ¹, Martin Hennecke ¹, Daniel Schick ¹, Clemens von Korff Schmising ^{1,*}, and Stefan Eisebitt ^{1,2}

¹Max-Born-Institut für Nichtlineare Optik und Kurzzeitspektroskopie, Max-Born-Straße 2A, 12489 Berlin, Germany

²Institut für Optik und Atomare Physik, Technische Universität Berlin, 10623 Berlin, Germany



(Received 9 February 2024; accepted 7 May 2024; published 30 May 2024)

Ultrafast transverse magneto-optical Kerr effect (T-MOKE) spectroscopy in the extreme ultraviolet spectral range provides element-specific information about the magnetization dynamics of complex magnetic structures. However, the relationship between the T-MOKE observable, denoted *magnetic asymmetry*, and the magnetization of a sample can exhibit significant nonlinearities, even in the case of magnetization changes that are homogeneous along the depth of the sample and without considering any nonequilibrium spin dynamics. Here, we combine static and time-resolved experimental data with simulations based on a wave propagation algorithm for a prototypical magnetic heterostructure that exhibits pronounced deviations from a linear relationship between magnetic asymmetry and magnetization, including *increasing* values of asymmetry in spite of a *reducing* magnetization. As an outlook, we describe sample structures and experimental geometries for which a linear response of the T-MOKE observable remains a valid approximation.

DOI: [10.1103/PhysRevB.109.184440](https://doi.org/10.1103/PhysRevB.109.184440)

I. INTRODUCTION

Measurements using transverse magneto-optical Kerr effect (T-MOKE) spectroscopy in the XUV spectral range have become an established method for the investigation of ultrafast magnetization dynamics in multicomponent materials and multilayer systems. T-MOKE is characterized by an asymmetry in the reflectance for two opposite magnetization directions aligned perpendicular to the reflection plane of the incident *p*-polarized radiation. This effect originates from the magnetic medium's finite off-diagonal elements in the dielectric tensor [1] and is strongly enhanced at an atomic resonance, thus providing element selectivity. The experimental geometry is shown schematically in Fig. 1: broadband XUV radiation, incident at the normal angle θ_i , is reflected off a magnetic sample and subsequently spectrally dispersed and detected by a camera. Ultrafast dynamics are recorded employing a pump-probe technique in which an optical laser pulse excites the sample at varying time delays before the XUV pulse probes the evolving magnetization of the sample.

In contrast to magnetic circular dichroism (MCD) experiments in transmission geometry [2,3], T-MOKE does not require circularly polarized light. This avoids additional experimental difficulties in controlling the polarization of the XUV radiation, either intrinsically within the high-harmonic generation (HHG) process itself [4–6], extrinsically via specialized optics [7,8], or by performing a polarization analysis [9–12]. Measurements in reflection geometry also allow investigating a wider range of samples, including systems grown on crystalline substrates, and

facilitate easier heat management in high-repetition rate, time-resolved pump-probe experiments. Furthermore, analysis of the time-dependent reflectance as a function of either the angle of incidence or photon energy allows obtaining detailed information on transient magnetization depth profiles [13,14].

Time-resolved T-MOKE measurements using radiation from high-harmonic generation sources were first successfully conducted by La-O-Vorakiat *et al.* [15] to investigate the ultrafast response of a permalloy sample after optical excitation. Further development of T-MOKE spectroscopy allowed tackling important questions regarding the microscopic origin of ultrafast magnetization dynamics. Attempts were made to disentangle and quantify contributions stemming from Stoner (reduction of exchange splitting) and Heisenberg (generation of magnons) excitations [16–18] and to track ultrafast superdiffusive spin transport in multilayer structures [19–21]. Recently, MCD [3,22] as well as T-MOKE [23–25] experiments in the XUV spectral range provided the first experimental evidence of optical intersite spin transfer, a process theoretically predicted by Dewhurst *et al.* [26] in 2018. Here, spins are transferred between two sublattices by the optical excitation itself, while the efficiency and the direction of the transfer are dictated by the availability of empty states above the Fermi energy. In the T-MOKE experiments an increase of magnetic asymmetry at certain photon energies was interpreted as an increase of magnetization at the corresponding sublattices upon laser excitation.

However, from the very beginning T-MOKE experiments have attracted a considerable amount of criticism because the reflectance of a laser-excited magnetic film can, in principle, be influenced by distinct changes in the real and imaginary parts of the nonmagnetic [27–29] as well as magnetic [30] index of refraction. The controversy was further fueled

*korff@mbi-berlin.de

by conflicting demagnetization time constants of Fe and Ni obtained from L -edge MCD transmission experiments [31] and XUV T-MOKE measurements [32], as well as by the difficulty in reproducing T-MOKE results, showing an enhancement of the Fe magnetization in interlayer coupled Fe/Ni systems [16], in L -edge MCD transmission experiments [33]. The work by Jana *et al.* [34] is important in this respect since it provides the first systematic comparison between L -edge MCD and M -edge T-MOKE. Here, a delayed onset of the demagnetization of Ni in FeNi alloys, previously observed in a number of T-MOKE experiments [32,35], was confirmed employing both techniques.

Finally, the T-MOKE observable is generally assumed to be directly proportional to the magnetization, an approximation, however, which is derived for the case of a small magnetic contribution to the total reflectance and for a single vacuum/magnetic layer interface. In this work, we scrutinize this assumption by investigating the relationship between magnetic asymmetry and magnetization for realistic sample structures and common experimental geometries. To achieve this objective, we compare static and time-resolved measurements with detailed simulations using a wave propagation matrix formalism taking into account reflection and refraction at each interface. We demonstrate that particularly for measurements performed in the vicinity of the Brewster angle around 45° , where the T-MOKE observable is maximized but at the same time the nonmagnetic reflectance is minimized, pronounced deviations from a direct proportionality between asymmetry and magnetization arise. We emphasize that this is already the case for the simplest scenario, where the magnetization decreases homogeneously within the probed sample volume and without considering any specific excited state or nonequilibrium demagnetization dynamics. Finally, we lay out strategies to retain a linear relationship between T-MOKE measurements and magnetization.

II. T-MOKE ASYMMETRY

In the following, we present a brief derivation of the commonly used approximation for the T-MOKE asymmetry at a single vacuum/magnetic sample interface. We start by separating the nonmagnetic r_p^n and magnetic r_p^m reflection coefficients:

$$\begin{aligned} r_p^n &= \frac{n \cos \theta_i - \cos \theta_t}{n \cos \theta_i + \cos \theta_t}, \\ r_p^m &= \frac{2inQ \cos \theta_i \sin \theta_t}{(n \cos \theta_i + \cos \theta_t)^2}, \end{aligned} \quad (1)$$

where n is the refractive index of the magnetic layer, $\theta_{i,t}$ are the normal incidence and refracted angles, respectively, and Q describes the magneto-optical constant, which is proportional to the magnetization M [1]. The magnetic asymmetry is defined as the difference between the reflectances for the two magnetization directions R_p^\pm , normalized to their sum:

$$A = \frac{R_p^+ - R_p^-}{R_p^+ + R_p^-} = \frac{|r_p^n + r_p^m|^2 - |r_p^n - r_p^m|^2}{|r_p^n + r_p^m|^2 + |r_p^n - r_p^m|^2}. \quad (2)$$

Rewriting A using the identity $z + z^* = 2\text{Re}(z)$, where $\text{Re}(\cdot)$ denotes the real part of the complex quantity and $*$ represents

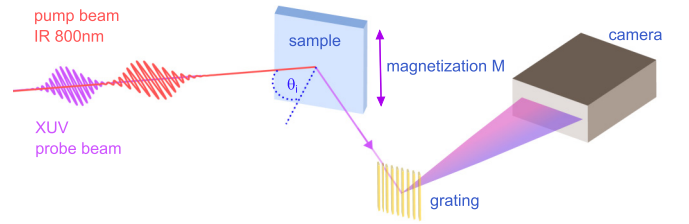


FIG. 1. Schematic of the transverse magneto-optical Kerr effect (T-MOKE) geometry. A p -polarized, ultrashort, and broadband XUV pulse impinges on the sample at the normal angle θ_i , and the reflected spectrum is detected by a spectrometer, consisting of a grating and a camera. The magnetization M of the sample is set perpendicular to the plane of incidence.

its complex conjugate, yields

$$A = \frac{2\text{Re}(r_p^n \cdot r_p^{m*})}{|r_p^n|^2 + |r_p^m|^2} = 2\text{Re}\left(\frac{r_p^m}{r_p^n}\right) \underbrace{\left(\frac{1}{1 + \frac{|r_p^m|^2}{|r_p^n|^2}}\right)}_{\mathfrak{T}_2}. \quad (3)$$

We now approximate the expression by a Taylor expansion of the second term \mathfrak{T}_2 around $|r_p^m|^2/|r_p^n|^2 = 0$ and retain only the zero-order term, yielding the following expression:

$$A_{\text{app}} \approx 2\text{Re}\left(\frac{r_p^m}{r_p^n}\right) \left(1 - \frac{|r_p^m|^2}{|r_p^n|^2}\right) \approx 2\text{Re}\left(\frac{r_p^m}{r_p^n}\right). \quad (4)$$

Plugging in the reflection coefficients $r_p^{n,m}$, we reach the approximation that is generally used to relate measured magnetic asymmetries to the magnetization:

$$A_{\text{app}} \approx 2\text{Re}\left(\frac{\epsilon_{xy} \sin 2\theta_i}{n^4 \cos^2 \theta_i - n^2 + \sin^2 \theta_i}\right) \propto M, \quad (5)$$

where $\epsilon_{xy} = iQn^2$ is the off-diagonal elements of the dielectric function. As $n \approx 1$ in the XUV spectral range, the asymmetry is maximized for $\theta_i \approx 45^\circ$, i.e., at the Brewster angle θ_B . We can readily test the validity of the approximation by calculating the second term \mathfrak{T}_2 of Eq. (3). As examples, we choose a vacuum/Fe interface and a vacuum/Ni interface, calculate $\epsilon_{xy} = 2in(\Delta\delta - i\Delta\beta)$, and use tabulated values for n [36] as well as for $\Delta\delta$ and $\Delta\beta$ [37,38]. In Fig. 2, we display the results as a function of both the incidence angle θ_i and photon energy E_{ph} . In the vicinity of the Brewster angle, the prerequisite of the approximation $|r_p^m| \ll |r_p^n|$ is no longer valid, leading to values $\mathfrak{T}_2 \ll 1$. Within the θ_i - E_{ph} map, shown in Fig. 2, we find minimum values of $\mathfrak{T}_2 = 0.06$ and 0.60 for Fe and Ni, respectively. We also note that for experimental conditions where \mathfrak{T}_2 is significantly less than 1, the approximated asymmetry A_{app} reaches values exceeding ± 1 , which is inconsistent with a normalized quantity. Obviously, care must be taken when using expression (5) to characterize magnetic asymmetries in T-MOKE experiments. While these limitations were discussed in some detail in the Ph.D. thesis of Turgut [39], we emphasize that, with the majority of T-MOKE experiments having been performed in the vicinity of the Brewster angle, this important aspect has not been given sufficient attention.

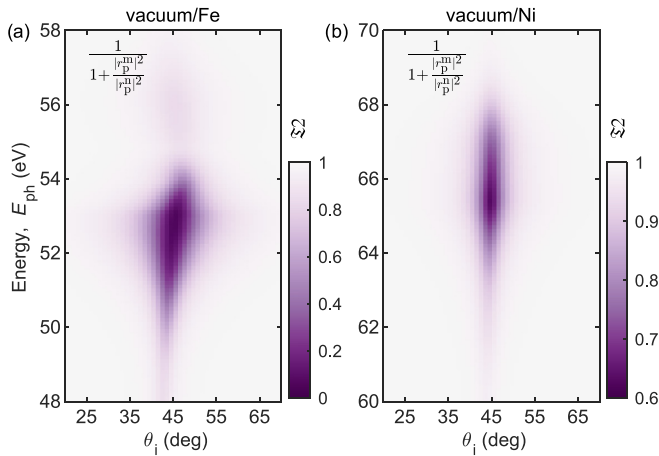


FIG. 2. Calculated term $\mathfrak{A}2$ as a function of the incidence angle θ_i and photon energy E_{ph} , describing the deviation between A and A_{app} for (a) a vacuum/Fe interface and (b) a vacuum/Ni interface. In the vicinity of the Brewster angle, $\mathfrak{A}2$ reaches values significantly less than 1. Note that the color maps are scaled differently in the two panels.

The second approximation in Eq. (5) limits the analysis of A to a *single* vacuum/magnetic interface. This is generally not fulfilled because even experimental studies of magnetic monolayers are effectively complex heterostructures, as thin film samples often rely on seed layers on a substrate to tune their magnetic properties, and are also often covered by a capping layer to prevent oxidation. Additionally, in time-resolved experiments, where the magnetic layer is optically excited, the layer thickness of the magnetic film is deliberately limited to the optical penetration depth of the pump pulse of approximately 10–15 nm in order to avoid depth-dependent excitation profiles. In this common situation, the reflectance of the XUV probe pulse is also influenced by the interfaces between the magnetic film and the seed layer and between the seed layer and the substrate. In these cases, the T-MOKE asymmetry can be calculated by simulating the reflectance of the investigated sample heterostructure using the well-established matrix formalism first introduced by Parratt [40] and later extended to describe magnetic systems [41–43]. Here, one solves the wave field while taking into account the Fresnel equations and using a recursive algorithm to describe multibeam interference from complex structures with multiple interfaces or density and magnetization gradients. In this work, we use an implementation provided by the UDKM1DSIM toolbox [44]. We note that the main additional challenge to achieve reliable results in such calculations is connected to accurate knowledge of the sample structure, i.e., the layer thicknesses, densities, interface roughnesses, and surface oxidation, as well as of the exact values of the atomic and magnetic form factors at the investigated resonances.

III. EXAMPLE STRUCTURE

A. Static characterization

In the following, we present experimental T-MOKE measurements in which both assumptions leading to the linear relationship between magnetic asymmetry and magnetization

are violated; i.e., the magnetic reflectance dominates for certain photon energies and incidence angles, and the reflectance is not given by a single vacuum/magnetic film interface. We present calculations based on the above-mentioned matrix formalism that demonstrate pronounced nonlinearities between changes in the magnetization of a magnetic heterostructure and corresponding changes in the magnetic asymmetry, i.e., $A \not\propto M$.

The investigated sample structure Al(30 nm)/Fe₅₀Ni₅₀(5 nm)/Ta(2 nm)/glass is grown via electron beam evaporation on a glass substrate. The Ta layer acts as a seed layer for the growth process, while the Al layer prevents oxidation. We emphasize that due to the small absorption cross section of Al for energies below its L edge, the relatively large thickness of the Al capping layer has an almost negligible influence on the reflectance in the XUV spectral range. The FeNi alloy exhibits an in-plane magnetization with a square hysteresis loop, characterized by a small coercive field less than 10 mT.

The measurements are performed using XUV radiation with a photon energy between 45 and 72 eV, generated by a HHG source. We focus laser pulses from a Ti:sapphire based amplifier system with a pulse duration of 25 fs, a repetition rate of 3 kHz, a pulse energy of ≈ 2.5 mJ, and a center wavelength of $\lambda = 800$ nm into a gas cell filled with helium. Depending on the setting of the chirp and energy of the laser pulses, either the resulting XUV spectrum is characterized by discrete narrow-bandwidth emission peaks, separated by ≈ 3.1 eV, or it is quasicontinuous. To determine the magnetic asymmetry, an electromagnet toggles the magnetization direction of the sample between the two opposite directions perpendicular to the plane of incidence, yielding the reflectances R_p^\pm . For more details on the experimental setup and time-resolved techniques, we refer to Refs. [45,46].

Figure 3(a) displays the reflectance measured by eight discrete harmonic emission peaks for the two magnetization directions of the FeNi alloy, as well as the magnetic asymmetry measured using a continuous XUV spectrum (solid green line) in the energy range of the Fe and Ni $M_{3,2}$ resonances. We observe large asymmetry values with a bipolar shape almost approaching $\pm 100\%$ for Fe around 54 eV and up to 50% for Ni around 67 eV. The dots indicate photon energies of harmonics H33, H35, and H39, for which we will later discuss time-resolved data (see Sec. III B).

The dashed violet line in Fig. 3(a) indicates the simulated magnetic asymmetry obtained from the wave propagation algorithm implemented by the UDKM1DSIM toolbox. The complex atomic and magnetic form factors are retrieved from the tabulated values provided by Henke *et al.* [36], complemented by MCD and Faraday measurements for the M -edge resonance of Fe and Ni [37,38]. The thicknesses of the different layers are determined during the growth process by a quartz crystal microbalance, calibrated by atomic force microscopy. To yield good agreement between simulated and experimental asymmetry, we allow small variations of the absolute values of the elemental magnetic moments. We also use a reduced density of Ta, in very close agreement with tabulated density values of Ta(V) oxide, suggesting a partial oxidation of the evaporation target. This is consistent with previous work in the literature [47,48] and by us, in which we confirmed the

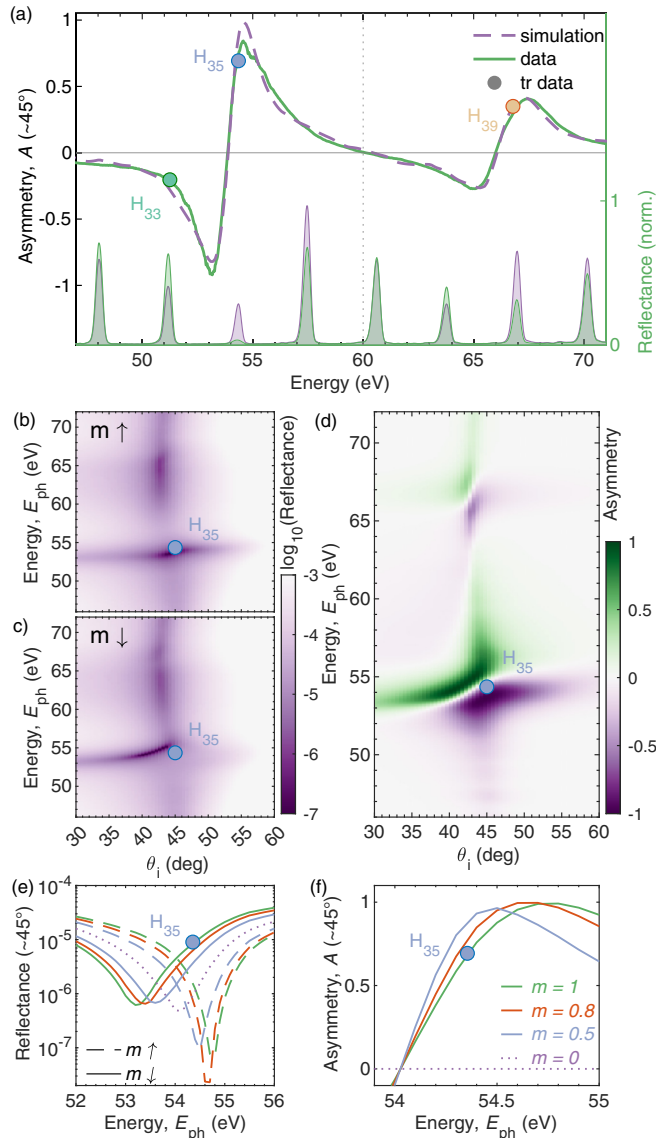


FIG. 3. (a) Measured (solid green line) and simulated (dashed purple line) continuous spectra of the magnetic asymmetry, as well as measured reflectance of the discrete harmonic emission peaks for the two magnetization directions of the FeNi alloy in the photon energy range of the Fe and Ni $M_{3,2}$ resonance. The dots indicate the photon energies of HHG peaks $E_{H33} = 51.3$ eV, $E_{H35} = 54.4$ eV, and $E_{H39} = 66.8$ eV, for which we later discuss the ultrafast magnetization dynamics. (b) and (c) Simulations of the reflectance as a function of the photon energy E_{ph} and angle of incidence θ_i for both transverse magnetization directions. (d) Corresponding simulation of the magnetic asymmetry. (e) Reflectance at 45° around the Fe $M_{3,2}$ resonance for the $m \uparrow$ (dashed lines) and $m \downarrow$ (solid lines) magnetization directions, calculated for decreasing values of the magnetic moment. (f) Corresponding asymmetries, clearly showing a strongly nonlinear behavior at H35, where a decrease in magnetization leads to an increase in A .

reduced Ta density by independent hard x-ray reflectance measurements [14]. Finally, we assume that the top Al layer is oxidized and model this by a 2 nm thin Al_2O_3 layer [47]. We note that XUV reflectances and magnetic asymmetries are

especially sensitive to the oxidation of heavy elements since their densities are significantly reduced when oxidized.

The determined magnetic and structural properties of the FeNi system now allow us to calculate the reflectances for the two transverse magnetization directions as a function of both the incidence angle θ_i and photon energy E_{ph} . The results are shown on a logarithmic scale in Figs. 3(b) and 3(c). Around the Brewster angle, i.e., in the vicinity of 45° , the reflectance is strongly reduced and reaches values down to 1×10^{-7} . In this region we observe large differences in reflectance for the two opposite directions of magnetization, caused by changes in the dichroic index of refraction. This behavior is particularly pronounced for H35 at the Fe $M_{3,2}$ resonance and a clear indication that the magnetic contribution to the total reflectance starts to dominate. This is also reflected in the corresponding asymmetry map shown in Fig. 3(d), revealing the largest asymmetry amplitudes varying between negative and positive polarity around the Brewster angle and the $M_{3,2}$ resonance.

In order to examine the reflectance around the Brewster angle in more detail, we show line plots of the simulated spectra at $\theta_i = 45^\circ$ from 52 to 56 eV in Fig. 3(e). We observe pronounced minima of the reflectance, shifted for the two magnetization directions $m \uparrow$ (dashed lines) and $m \downarrow$ (solid lines) by approximately 1.2 eV. As we reduce the normalized magnetization $m = M/M_0$ of the FeNi alloy, the difference in the minimum reflectances decreases and, as expected, converges to a single value at ≈ 54 eV for $m = 0$ (violet dotted line). In this photon energy range, the linear approximation (5) evidently does not hold: the reflectance is strongly influenced by the magnetic part r_p^m . In Fig. 3(f), we turn again to the asymmetry A , showing its response at $\theta_i = 45^\circ$ and zoom in on the photon energy range between 54 and 55 eV, where the asymmetry is characterized by a very steep slope, increasing from 0 to almost 1. Strikingly, as we again examine the effect of a reduction of the magnetization, we calculate an increase in the magnetic asymmetry; compare the response of A as m is reduced from 1 (green line) to 0.8 (red line) and 0.5 (blue line). We again mark the photon energy of H35 at 53.4 eV, for which we measured time-resolved data. We note that for the case of a single vacuum/FeNi interface, we do not observe that the asymmetries for different values of m cross each other, suggesting that the complicated response is a direct consequence of the multilayer structure.

B. Time-resolved response

In the following, we present ultrafast demagnetization measurements which confirm our simulations regarding a nonlinear relationship between magnetic asymmetry and magnetization. We excite the sample with laser pulses with a wavelength of $\lambda = 800$ nm and a pulse duration below 30 fs at the sample position. The pump fluence is set to ≈ 39 mJ/cm², defined as the incident pulse energy divided by the effective footprint of the laser on the sample surface, calculated using the full width at half maximum of the Gaussian beam shape as the diameter. The light is almost exclusively absorbed within the Al layer, generating hot electrons which are injected into the FeNi alloy, causing its ultrafast loss of magnetization. This type of indirect excitation has been shown to

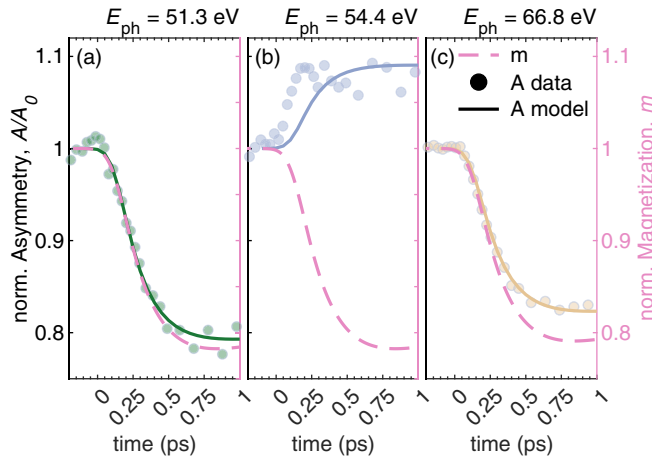


FIG. 4. Time-resolved magnetic asymmetry A/A_0 for the photon energies (a) $E_{H33} = 51.3$ eV, (b) $E_{H35} = 54.4$ eV, and (c) $E_{H39} = 66.8$ eV. The dashed pink line shows a single-exponential, spatially homogeneous decrease of the magnetization, while the solid lines displays the corresponding calculated magnetic asymmetry based on the wave propagation algorithm. For 54.4 eV, the magnetic asymmetry exhibits a strongly nonlinear relationship to magnetization.

lead to efficient and ultrafast magnetization dynamics [49,50]. Also see our very recent work on a direct comparison between direct and indirect excitation of an FeNi alloy [51].

The experimental results are summarized in Fig. 4 for the three photon energies marked in the static asymmetry spectra in Fig. 3(a). We show the measured normalized asymmetry $A(t)/A(t < 0) = A/A_0$ (dots) as a function of pump-probe delay up to 1 ps. To describe the data, we calculate the asymmetry for a normalized magnetization that decays exponentially with time but homogeneously along the depth of the sample according to

$$m = [1 - C(1 - e^{-t/\tau})]\Theta(t) * G(t). \quad (6)$$

Here, we additionally take into account the temporal resolution of the experiment of approximately 35 fs [45] by convolution with a Gaussian function $G(t)$. Θ is the Heaviside function at time delay zero. We then vary the amplitude C and time constant τ until the calculated asymmetry matches the measured data. We show the calculated asymmetry as a solid line and the corresponding magnetization as a pink dashed line. At $E_{ph} = 51.3$ eV, we find $\tau \approx 250$ fs and $C = 0.22$. Importantly, at this energy $A \propto M$ provides a very good approximation. The situation changes dramatically when we examine the response at 54.4 eV, shown in Fig. 4(b). Here, for the same evolution of m (pink dashed line), we observe an ultrafast increase of the measured asymmetry by about 7%, in agreement with the results shown in Fig. 3(f). We examine one further photon energy, now in resonance with Ni at 66.8 eV. Here, we again observe an exponential decay of the measured asymmetry. The calculated asymmetry, which describes the data [solid yellow line in Fig. 4(c)], corresponds to a very similar demagnetization amplitude compared to Fe and is shown again as a pink dashed line. We find $C = 0.21$ and $\tau \approx 180$ fs. Importantly, we find that the measured asymmetry and magnetization show a non-negligible absolute deviation of about 3%. Assuming direct proportionality between A and

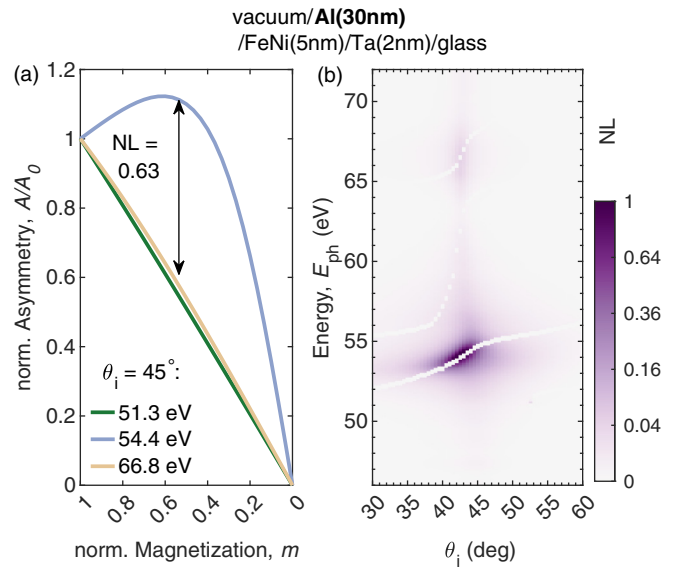


FIG. 5. (a) Normalized magnetic asymmetry A/A_0 for the sample Al(30 nm)/Fe₅₀Ni₅₀(5 nm)/Ta(2 nm)/glass as a function of magnetization calculated for an angle in the vicinity of the Brewster angle at $\theta_i = 45^\circ$. (b) The nonlinear response (NL) for the same sample as a function of normal incidence angles θ_i and photon energies E_{ph} . Note that the color map is scaled quadratically.

m , one would underestimate the relative demagnetization amplitude by more than 15%.

C. Quantifying the nonlinear response of the magnetic asymmetry

We now introduce a simple metric for the nonlinear response of the magnetic asymmetry as the magnetization is reduced for every point in space spanned by the incidence angles θ_i and photon energies E_{ph} . In order to do so, we first calculate the normalized asymmetry A/A_0 as a function of the normalized magnetization m for the experimental geometry discussed above, i.e., $\theta_i = 45^\circ$. We again consider only a reduction of the magnetization that is homogeneous along the depth of the FeNi alloy and, for simplicity, identical for both elements Fe and Ni. This allows us to compare the relationship between A/A_0 and m for the same three photon energies discussed above. Figure 5(a) summarizes the results. While we find a nearly perfect linear dependence for $E_{H33} = 51.3$ eV and only moderate deviations for $E_{H39} = 66.8$ eV, at $E_{H35} = 54.4$ eV the response strongly differs from the approximation $A/A_0 \propto m$. First, the asymmetry increases by about 15% for a magnetization amplitude of 0.6 before it crosses $A/A_0 = 1$ for $m = 0.37$ and finally drops to zero. It becomes apparent that this highly nonmonotonic and nonlinear dependence of the asymmetry on the magnetization not only influences the amplitude but also the perceived dynamics of the pump-induced change. As the slope of the asymmetry as a function of magnetization depends sensitively on the structural and magnetic parameters of the sample, this may offer a potential explanation for the observed discrepancy in the onset of measured and calculated time-resolved asymmetries at $E_{H35} = 54.4$ eV in Fig. 4(b). Furthermore, we note that the

very early dynamics may be influenced by more complicated nonequilibrium magnetization dynamics [18,30,45,52], which are not taken into account in our simulation.

To quantify the nonlinear response of the asymmetry for varying magnetization amplitudes, we introduce the metric NL, defined as the maximum difference between the linear function $A/A_0 = m$ and the actual, calculated values of $A(m)/A(m=1)$ (see Fig. 5). For $E_{H35} = 54.4$ eV, we find $NL = 0.63$; for $E_{H39} = 66.8$ eV we find a much smaller value of $NL = 0.04$. The values of NL as a function of both experimental parameters, i.e., the angle of incidence θ_i and photon energy E_{ph} , are summarized in Fig. 5(b) for the investigated sample structure Al(30 nm)/Fe₅₀Ni₅₀(5 nm)/Ta(2 nm)/glass. We find very large values around the Brewster angle, reaching values of up to $NL = 1.2$ around the Fe $M_{3,2}$ resonance. Note that in regions where A exhibits a zero crossing, NL has been set to zero.

IV. OPTIMIZED SAMPLE AND EXPERIMENTAL GEOMETRIES

In the final part of our study, we discuss strategies to avoid or minimize nonlinearities in optical-pump–XUV-probe T-MOKE experiments. It is important to note that although correcting for a nonlinear relationship between A/A_0 and m is possible in theory, reflectance simulations require precise knowledge of both the structural parameters and the magnetic and nonmagnetic indices of refraction. We find that particularly for very large values of NL found close to the Brewster angle, even small uncertainties in the input parameters can result in significant effects on the asymmetry, making numerical corrections difficult. To obtain a precise measure of the magnetization and its dynamics, it is thus advantageous to avoid such experimental geometries. Furthermore, a suitable choice of the material for the antioxidation cap layer can significantly change the situation.

In the design of an optimized sample structure, we are guided by the condition for which the approximation in Eq. (5) holds, namely, that the total reflectance has to be dominated by the nonmagnetic reflectivity, i.e., $|r_p^m| \ll |r_p^n|$. This suggests choosing a high-Z material as a capping layer to increase the nonmagnetic reflectivity, albeit at the cost of reduced magnetic asymmetry. As an example, we chose Ta instead of Al. To facilitate a direct comparison with the investigated Al-capped magnetic FeNi layer, we adopt the same sample parameters and replace only the capping layer by 2 nm of Ta. We assume a thin Ta oxide layer of 1.5 nm [47,48] and model it with tabulated values for Ta(V) oxide. Since oxidation of the top layer reduces its density and thus the nonmagnetic reflectance of the structure, the calculated values of NL can be considered an upper limit.

The magnetic asymmetry and NL landscape of the corresponding Ta(2 nm)/Fe₅₀Ni₅₀(5 nm)/Ta(2 nm)/glass sample are shown in Figs. 6(a) and 6(b), respectively. We still observe sizable values of the magnetic asymmetry, but now with negligible values of $NL < 2 \times 10^{-3}$.

To gain an overview of how capping layers (CLs) grown with different materials influence the asymmetry and NL values, we repeat the above simulations for the same magnetic heterostructure: CL(2 nm)/Fe₅₀Ni₅₀(5 nm) /Ta(2 nm)/glass.

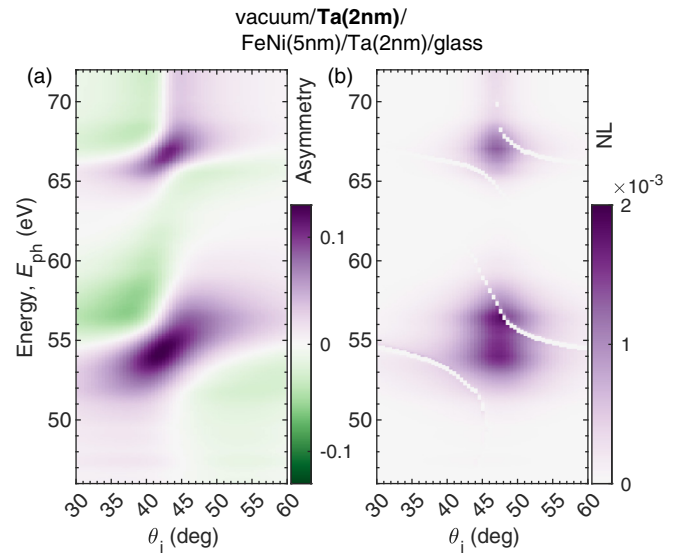


FIG. 6. (a) Magnetic asymmetry and (b) NL map as a function of the incidence angle θ_i and photon energy E_{ph} of the sample structure Ta(2 nm)/Fe₅₀Ni₅₀(5 nm)/Ta(2 nm)/glass. Note that changing the capping layer to a high-Z element significantly reduces the maximum values of the nonlinear response (NL).

For low-Z materials such as Al, SiN, MgO, and native oxide layers such as NiO, we find large maximum asymmetry amplitudes approaching 1, but accompanied by very large maximum values of $NL > 2$. These maxima are found in the vicinity of the Brewster angle and atomic resonances, where, evidently, the assumption of a linear relationship between asymmetry and magnetization completely breaks down. On the other hand, choosing a high-Z material as a capping layer, for example Pt, Ru, or Ta, allows recovering the linear relationship between magnetic asymmetry and magnetization. While we find significantly lower asymmetry amplitudes on the order of $A = 0.1$, the highest NL values remain below 0.01.

As the magnetic properties of the magnetic film can be strongly influenced by an adjacent layer, the choice of materials can be a constraint depending on the nature of the investigation. In particular, interfaces with a heavy metal can lead to perpendicular magnetic anisotropy [53] and spin-orbit torques [54] in the presence of currents in the sample. Interdiffusion can lead to magnetically dead layers near the interface, which is the case for Ta and Ru, for example [55,56]. Although platinum is a good element for oxidation protection, it forms a strong interfacial magnetization leading to overlapping magnetic asymmetries of its $O_{3,2}$ resonance in the spectral regions of the Fe and Co $M_{3,2}$ edges [46]. In these cases, as well as for low-Z capping materials and capping layers with an unknown oxidation state, it may be preferable to perform experiments away from the Brewster angle to ensure direct proportionality between asymmetry and magnetization.

V. CONCLUSION

We have discussed the limitations of the commonly used approximation of the T-MOKE observable, which predicts a direct proportionality between magnetic asymmetry and

magnetization. In the vicinity of the Brewster angle, deviations between the exact and approximated representations of A can exceed 100%, leading to potentially large errors in determining the demagnetization amplitude in time-resolved measurements. Furthermore, we showed that in magnetic heterostructures wave propagation and interference effects can significantly alter the reflectance and corresponding asymmetry, leading to a complex, nonmonotonic and nonlinear relationship between A/A_0 and m . We provided experimental results—both static and time resolved—in conjunction with simulations using a wave propagation matrix formalism for a prototypical magnetic heterostructure. Our most striking experimental observation is that for photon energies tuned to the Fe $M_{3,2}$ resonance and for measurements in the vicinity of the Brewster angle, the magnetic asymmetry *increases* in spite of a *decreasing* magnetization, indicating a clear breakdown of $A \propto M$. Our investigation of the relationship between

magnetic asymmetry and magnetization as a function of both the angle of incidence and photon energy suggests two strategies to avoid a nonlinear T-MOKE response, albeit at the cost of a lower magnetic asymmetry: One should perform the measurement away from the Brewster angle and/or cap the magnetic films with a high- Z material, such as Ta, Pt, or Ru. Both approaches increase the nonmagnetic part of the total reflectance and allow retaining a linear relationship between magnetic asymmetry and magnetization.

ACKNOWLEDGMENTS

C.v.K.S., J.R., and S.E. acknowledge financial support from the Deutsche Forschungsgemeinschaft (DFG, German Research Foundation), Project ID No. 328545488, TRR 227, Project No. A02.

-
- [1] P. Oppeneer, Magneto-optical Kerr spectra, in *Handbook of Magnetic Materials* (Elsevier, Amsterdam, 2001), Vol. 13, pp. 229–422.
- [2] F. Willems, C. T. L. Smeenk, N. Zhavoronkov, O. Kornilov, I. Radu, M. Schmidbauer, M. Hanke, C. von Korff Schmising, M. J. J. Vrakking, and S. Eisebitt, Probing ultrafast spin dynamics with high-harmonic magnetic circular dichroism spectroscopy, *Phys. Rev. B* **92**, 220405(R) (2015).
- [3] F. Siegrist, J. A. Gessner, M. Osslander, C. Denker, Y.-P. Chang, M. C. Schröder, A. Guggenmos, Y. Cui, J. Walowski, U. Martens, J. K. Dewhurst, U. Kleineberg, M. Münzenberg, S. Sharma, and M. Schultze, Light-wave dynamic control of magnetism, *Nature (London)* **571**, 240 (2019).
- [4] O. Kfir, P. Grychtol, E. Turgut, R. Knut, D. Zusin, D. Popmintchev, T. Popmintchev, H. Nembach, J. M. Shaw, A. Fleischer, H. Kapteyn, M. Murnane, and O. Cohen, Generation of bright phase-matched circularly-polarized extreme ultraviolet high harmonics, *Nat. Photon.* **9**, 99 (2015).
- [5] T. Fan *et al.*, Bright circularly polarized soft x-ray high harmonics for x-ray magnetic circular dichroism, *Proc. Natl. Acad. Sci. USA* **112**, 14206 (2015).
- [6] G. Lambert, B. Vodungbo, J. Gautier, B. Mahieu, V. Malka, S. Sebban, P. Zeitoun, J. Luning, J. Perron, A. Andreev, S. Stremoukhov, F. Ardana-Lamas, A. Dax, C. P. Hauri, A. Sardinha, and M. Fajardo, Towards enabling femtosecond helicity-dependent spectroscopy with high-harmonic sources, *Nat. Commun.* **6**, 6167 (2015).
- [7] B. Vodungbo, A. Barszczak Sardinha, J. Gautier, G. Lambert, C. Valentin, M. Lozano, G. Iaquaniello, F. Delmotte, S. Sebban, J. Luning, and P. Zeitoun, Polarization control of high order harmonics in the EUV photon energy range, *Opt. Express* **19**, 4346 (2011).
- [8] C. von Korff Schmising, D. Weder, T. Noll, B. Pfau, M. Hennecke, C. Strüber, I. Radu, M. Schneider, S. Staack, C. M. Günther, J. Luning, A. el dine Merhe, J. Buck, G. Hartmann, J. Viehhaus, R. Treusch, and S. Eisebitt, Generating circularly polarized radiation in the extreme ultraviolet spectral range at the free-electron laser FLASH, *Rev. Sci. Instrum.* **88**, 053903 (2017).
- [9] S. Yamamoto *et al.*, Ultrafast spin-switching of a ferrimagnetic alloy at room temperature traced by resonant magneto-optical Kerr effect using a seeded free electron laser, *Rev. Sci. Instrum.* **86**, 083901 (2015).
- [10] K. Yamamoto, S. E. Moussaoui, Y. Hirata, S. Yamamoto, Y. Kubota, S. Owada, M. Yabashi, T. Seki, K. Takahashi, I. Matsuda, and H. Wadati, Element-selectively tracking ultrafast demagnetization process in Co/Pt multilayer thin films by the resonant magneto-optical Kerr effect, *Appl. Phys. Lett.* **116**, 172406 (2020).
- [11] C. von Korff Schmising *et al.*, Element-specific magnetization dynamics of complex magnetic systems probed by ultrafast magneto-optical spectroscopy, *Appl. Sci.* **10**, 7580 (2020).
- [12] C. Alves, G. Lambert, V. Malka, M. Hehn, G. Malinowski, M. Hennes, V. Chardonnet, E. Jal, J. Luning, and B. Vodungbo, Resonant Faraday effect using high-order harmonics for the investigation of ultrafast demagnetization, *Phys. Rev. B* **100**, 144421 (2019).
- [13] V. Chardonnet, M. Hennes, R. Jarrier, R. Delaunay, N. Jaouen, M. Kuhlmann, N. Ekanayake, C. Léveillé, C. von Korff Schmising, D. Schick, K. Yao, X. Liu, G. S. Chiužbaian, J. Luning, B. Vodungbo, and E. Jal, Toward ultrafast magnetic depth profiling using time-resolved x-ray resonant magnetic reflectivity, *Struct. Dyn.* **8**, 034305 (2021).
- [14] M. Hennecke, D. Schick, T. Sidiropoulos, F. Willems, A. Heilmann, M. Bock, L. Ehrentraut, D. Engel, P. Hensing, B. Pfau, M. Schmidbauer, A. Furchner, M. Schnuerer, C. von Korff Schmising, and S. Eisebitt, Ultrafast element- and depth-resolved magnetization dynamics probed by transverse magneto-optical Kerr effect spectroscopy in the soft x-ray range, *Phys. Rev. Res.* **4**, L022062 (2022).
- [15] C. La-O-Vorakiat, M. Siemens, M. M. Murnane, H. C. Kapteyn, S. Mathias, M. Aeschlimann, P. Grychtol, R. Adam, C. M. Schneider, J. M. Shaw, H. Nembach, and T. J. Silva, Ultrafast demagnetization dynamics at the M edges of magnetic elements observed using a tabletop high-harmonic soft X-ray source, *Phys. Rev. Lett.* **103**, 257402 (2009).
- [16] E. Turgut, D. Zusin, D. Legut, K. Carva, R. Knut, J. M. Shaw, C. Chen, Z. Tao, H. T. Nembach, T. J. Silva, S.

- Mathias, M. Aeschlimann, P. M. Oppeneer, H. C. Kapteyn, M. M. Murnane, and P. Grychtol, Stoner versus Heisenberg: Ultrafast exchange reduction and magnon generation during laser-induced demagnetization, *Phys. Rev. B* **94**, 220408(R) (2016).
- [17] D. Zusin, P. M. Tengdin, M. Gopalakrishnan, C. Gentry, A. Blonsky, M. Gerrity, D. Legut, J. M. Shaw, H. T. Nembach, T. J. Silva, P. M. Oppeneer, H. C. Kapteyn, and M. M. Murnane, Direct measurement of the static and transient magneto-optical permittivity of cobalt across the entire M -edge in reflection geometry by use of polarization scanning, *Phys. Rev. B* **97**, 024433 (2018).
- [18] S. Jana, R. S. Malik, Y. O. Kvashnin, I. L. M. Locht, R. Knut, R. Stefanuik, I. Di Marco, A. N. Yaresko, M. Ahlberg, J. Åkerman, R. Chimata, M. Battiato, J. Söderström, O. Eriksson, and O. Karis, Analysis of the linear relationship between asymmetry and magnetic moment at the M edge of $3d$ transition metals, *Phys. Rev. Res.* **2**, 013180 (2020).
- [19] D. Rudolf, C. La-O-Vorakiat, M. Battiato, R. Adam, J. M. Shaw, E. Turgut, P. Maldonado, S. Mathias, P. Grychtol, H. T. Nembach, T. J. Silva, M. Aeschlimann, H. C. Kapteyn, M. M. Murnane, C. M. Schneider, and P. M. Oppeneer, Ultrafast magnetization enhancement in metallic multilayers driven by superdiffusive spin current, *Nat. Commun.* **3**, 1037 (2012).
- [20] E. Turgut, C. La-o-vorakiat, J. M. Shaw, P. Grychtol, H. T. Nembach, D. Rudolf, R. Adam, M. Aeschlimann, C. M. Schneider, T. J. Silva, M. M. Murnane, H. C. Kapteyn, and S. Mathias, Controlling the competition between optically induced ultrafast spin-flip scattering and spin transport in magnetic multilayers, *Phys. Rev. Lett.* **110**, 197201 (2013).
- [21] R. Gupta, F. Cosco, R. S. Malik, X. Chen, S. Saha, A. Ghosh, T. Pohlmann, J. R. L. Mardegan, S. Francoual, R. Stefanuik, J. Söderström, B. Sanyal, O. Karis, P. Svedlindh, P. M. Oppeneer, and R. Knut, Element-resolved evidence of superdiffusive spin current arising from ultrafast demagnetization process, *Phys. Rev. B* **108**, 064427 (2023).
- [22] F. Willems, C. von Korff Schmising, C. Strüber, D. Schick, D. W. Engel, J. K. Dewhurst, P. Elliott, S. Sharma, and S. Eisebitt, Optical inter-site spin transfer probed by energy and spin-resolved transient absorption spectroscopy, *Nat. Commun.* **11**, 871 (2020).
- [23] M. Hofherr, S. Häuser, J. K. Dewhurst, P. Tengdin, S. Sakshath, H. T. Nembach, S. T. Weber, J. M. Shaw, T. J. Silva, H. C. Kapteyn, M. Cinchetti, B. Rethfeld, M. M. Murnane, D. Steil, B. Stadtmüller, S. Sharma, M. Aeschlimann, and S. Mathias, Ultrafast optically induced spin transfer in ferromagnetic alloys, *Sci. Adv.* **6**, eaay8717 (2020).
- [24] P. Tengdin, C. Gentry, A. Blonsky, D. Zusin, M. Gerrity, L. Hellbrück, M. Hofherr, J. Shaw, Y. Kvashnin, E. K. Delczeg-Czirjak, M. Arora, H. Nembach, T. J. Silva, S. Mathias, M. Aeschlimann, H. C. Kapteyn, D. Thonig, K. Koumpouras, O. Eriksson, and M. M. Murnane, Direct light-induced spin transfer between different elements in a spintronic Heusler material via femtosecond laser excitation, *Sci. Adv.* **6**, eaaz1100 (2020).
- [25] S. A. Ryan, P. C. Johnsen, M. F. Elhanoty, A. Grafov, N. Li, A. Delin, A. Markou, E. Lesne, C. Felsner, O. Eriksson, H. C. Kapteyn, O. Grånäs, and M. M. Murnane, Optically controlling the competition between spin flips and intersite spin transfer in a Heusler half-metal on sub-100-fs time scales, *Sci. Adv.* **9**, eadi1428 (2023).
- [26] J. K. Dewhurst, P. Elliott, S. Shallcross, E. K. U. Gross, and S. Sharma, Laser-induced intersite spin transfer, *Nano Lett.* **18**, 1842 (2018).
- [27] C. La-O-Vorakiat, E. Turgut, C. A. Teale, H. C. Kapteyn, M. M. Murnane, S. Mathias, M. Aeschlimann, C. M. Schneider, J. M. Shaw, H. T. Nembach, and T. J. Silva, Ultrafast demagnetization measurements using extreme ultraviolet light: Comparison of electronic and magnetic contributions, *Phys. Rev. X* **2**, 011005 (2012).
- [28] B. Vodungbo, J. Gautier, G. Lambert, P. Zeitoun, and J. Lüning, Comment on “Ultrafast demagnetization measurements using extreme ultraviolet light: Comparison of electronic and magnetic contributions,” *Phys. Rev. X* **3**, 038001 (2013).
- [29] E. Turgut, P. Grychtol, C. La-O-Vorakiat, D. E. Adams, H. C. Kapteyn, M. M. Murnane, S. Mathias, M. Aeschlimann, C. M. Schneider, J. M. Shaw, H. T. Nembach, and T. J. Silva, Reply to “Comment on ‘Ultrafast demagnetization measurements using extreme ultraviolet light: Comparison of electronic and magnetic contributions,’” *Phys. Rev. X* **3**, 038002 (2013).
- [30] H. Probst, C. Möller, M. Schumacher, T. Brede, J. K. Dewhurst, M. Reutzler, D. Steil, S. Sharma, G. S. M. Jansen, and S. Mathias, Unraveling femtosecond spin and charge dynamics with extreme ultraviolet transverse MOKE spectroscopy, *Phys. Rev. Res.* **6**, 013107 (2024).
- [31] I. Radu, C. Stamm, A. Eschenlohr, F. Radu, R. Abrudan, K. Vahaplar, T. Kachel, N. Pontius, R. Mitzner, K. Hollmack, A. Föhlisch, T. A. Ostler, J. H. Mentink, R. F. L. Evans, R. W. Chantrell, A. Tsukamoto, A. Itoh, A. Kirilyuk, A. V. Kimel, and T. Rasing, Ultrafast and distinct spin dynamics in magnetic alloys, *SPIN* **05**, 1550004 (2015).
- [32] S. Mathias, C. La-O-Vorakiat, P. Grychtol, P. Granitzka, E. Turgut, J. M. Shaw, R. Adam, H. T. Nembach, M. E. Siemens, S. Eich, C. M. Schneider, T. J. Silva, M. Aeschlimann, M. M. Murnane, and H. C. Kapteyn, Probing the timescale of the exchange interaction in a ferromagnetic alloy, *Proc. Natl. Acad. Sci. USA* **109**, 4792 (2012).
- [33] A. Eschenlohr, L. Persichetti, T. Kachel, M. Gabureac, P. Gambardella, and C. Stamm, Spin currents during ultrafast demagnetization of ferromagnetic bilayers, *J. Phys.: Condens. Matter* **29**, 384002 (2017).
- [34] S. Jana, R. Knut, S. Muralidhar, R. S. Malik, R. Stefanuik, J. Åkerman, O. Karis, C. Schüßler-Langeheine, and N. Pontius, Experimental confirmation of the delayed Ni demagnetization in FeNi alloy, *Appl. Phys. Lett.* **120**, 102404 (2022).
- [35] S. Jana, J. A. Terschlüsen, R. Stefanuik, S. Plogmaker, S. Troisi, R. S. Malik, M. Svanqvist, R. Knut, J. Söderström, and O. Karis, A setup for element specific magnetization dynamics using the transverse magneto-optic Kerr effect in the energy range of 30-72 eV, *Rev. Sci. Instrum.* **88**, 033113 (2017).
- [36] B. Henke, E. Gullikson, and J. Davis, X-ray interactions: Photoabsorption, scattering, transmission, and reflection at $E = 50$ -30,000 eV, $Z = 1$ -92, *At. Data Nucl. Data Tables* **54**, 181 (1993).
- [37] S. Valencia, A. Gaupp, W. Gudat, H.-C. Mertins, P. M. Oppeneer, D. Abramsohn, and C. M. Schneider, Faraday

- rotation spectra at shallow core levels: $3p$ edges of Fe, Co, and Ni, *New J. Phys.* **8**, 254 (2006).
- [38] F. Willems, S. Sharma, C. v. Korff Schmising, J. K. Dewhurst, L. Salemi, D. Schick, P. Hessing, C. Strüber, W. D. Engel, and S. Eisebitt, Magneto-optical functions at the $3p$ resonances of Fe, Co, and Ni: *Ab initio* description and experiment, *Phys. Rev. Lett.* **122**, 217202 (2019).
- [39] E. Turgut, Studying laser-induced spin currents using ultrafast extreme ultraviolet light, Ph.D. thesis, University of Colorado Boulder, 2014.
- [40] L. G. Parratt, Surface studies of solids by total reflection of x-rays, *Phys. Rev.* **95**, 359 (1954).
- [41] J. Zak, E. Moog, C. Liu, and S. Bader, Universal approach to magneto-optics, *J. Magn. Magn. Mater.* **89**, 107 (1990).
- [42] M. Elzo, E. Jal, O. Bunau, S. Grenier, Y. Joly, A. Ramos, H. Tolentino, J. Tonnerre, and N. Jaouen, X-ray resonant magnetic reflectivity of stratified magnetic structures: Eigenwave formalism and application to a W/Fe/W trilayer, *J. Magn. Magn. Mater.* **324**, 105 (2012).
- [43] S. Macke and E. Goering, Magnetic reflectometry of heterostructures, *J. Phys.: Condens. Matter* **26**, 363201 (2014).
- [44] D. Schick, udkm1Dsim – A Python toolbox for simulating 1D ultrafast dynamics in condensed matter, *Comput. Phys. Commun.* **266**, 108031 (2021).
- [45] K. Yao, F. Willems, C. von Korff Schmising, I. Radu, C. Strber, D. Schick, D. Engel, A. Tsukamoto, J. K. Dewhurst, S. Sharma, and S. Eisebitt, Distinct spectral response in M -edge magnetic circular dichroism, *Phys. Rev. B* **102**, 100405 (2020).
- [46] C. von Korff Schmising, S. Jana, K. Yao, M. Hennecke, P. Scheid, S. Sharma, M. Viret, J.-Y. Chauleau, D. Schick, and S. Eisebitt, Ultrafast behavior of induced and intrinsic magnetic moments in CoFeB/Pt bilayers probed by element-specific measurements in the extreme ultraviolet spectral range, *Phys. Rev. Res.* **5**, 013147 (2023).
- [47] K. R. Lawless, The oxidation of metals, *Rep. Prog. Phys.* **37**, 231 (1974).
- [48] L. Gan, Jr., R. D. Gomez, C. J. Powell, R. D. McMichael, P. J. Chen, and W. F. Egelhoff, Thin Al, Au, Cu, Ni, Fe, and Ta films as oxidation barriers for Co in air, *J. Appl. Phys.* **93**, 8731 (2003).
- [49] B. Vodungbo *et al.*, Indirect excitation of ultrafast demagnetization, *Sci. Rep.* **6**, 18970 (2016).
- [50] N. Berggaard, M. Hehn, S. Mangin, G. Lengaigne, F. Montaigne, M. L. M. Lalieu, B. Koopmans, and G. Malinowski, Hot-electron-induced ultrafast demagnetization in Co/Pt multilayers, *Phys. Rev. Lett.* **117**, 147203 (2016).
- [51] C. von Korff Schmising, S. Jana, O. Züllich, D. Sommer, and S. Eisebitt, Direct versus indirect excitation of ultrafast magnetization dynamics in FeNi alloys, *Phys. Rev. Res.* **6**, 013270 (2024).
- [52] B. Rösner *et al.*, Simultaneous two-color snapshot view on ultrafast charge and spin dynamics in a Fe-Cu-Ni tri-layer, *Struct. Dyn.* **7**, 054302 (2020).
- [53] K. Yakushiji, T. Saruya, H. Kubota, A. Fukushima, T. Nagahama, S. Yuasa, and K. Ando, Ultrathin Co/Pt and Co/Pd superlattice films for MgO-based perpendicular magnetic tunnel junctions, *Appl. Phys. Lett.* **97**, 232508 (2010).
- [54] S. Emori, U. Bauer, S.-M. Ahn, E. Martinez, and G. S. D. Beach, Current-driven dynamics of chiral ferromagnetic domain walls, *Nat. Mater.* **12**, 611 (2013).
- [55] M. Kowalewski, W. H. Butler, N. Moghadam, G. M. Stocks, T. C. Schulthess, K. J. Song, J. R. Thompson, A. S. Arrott, T. Zhu, J. Drewes, R. R. Katti, M. T. McClure, and O. Escorcia, The effect of Ta on the magnetic thickness of permalloy ($\text{Ni}_{81}\text{Fe}_{19}$) films, *J. Appl. Phys.* **87**, 5732 (2000).
- [56] Y.-H. Wang, W.-C. Chen, S.-Y. Yang, K.-H. Shen, C. Park, M.-J. Kao, and M.-J. Tsai, Interfacial and annealing effects on magnetic properties of CoFeB thin films, *J. Appl. Phys.* **99**, 08M307 (2006).